CHAPTER 11

Simulating Biomass Fast Pyrolysis at the Single Particle Scale

PETER N. CIESIELSKI*[a], GAVIN M. WIGGINS[b], JOSEPH E. JAKES[c] AND C. STUART DAW[b]

[a]Biosciences Center, National Renewable Energy Laboratory, 15013 Denver W. Parkway, Golden, CO 80401, United States; [b]Oak Ridge National Laboratory, 2360 Cherahala Blvd., Knoxville, TN 37932, United States; [c]Forest Biopolymers Science and Engineering, USDA Forest Service Forest Products Laboratory, One Gifford Pinchot Drive, Madison, Wisconsin, United States 53726
*E-mail: peter.ciesielski@nrel.gov

11.1 Introduction

Biomass holds tremendous potential as a renewable feedstock for the production of fuels and chemicals. However, significant technological advancement is required before production of biofuels and bio-based chemicals will become widespread and economically self-sustaining at the industrial scale. Many of the greatest challenges surrounding biomass conversion stem from the complex nature of the feedstock. Biomass consists of the remains of once-living plant tissue, and therefore retains many of the characteristics of the original organism. These characteristics, such as microstructure, biopolymer composition, and mineral content, are species-specific and can vary

Green Chemistry Series No. 50
Fast Pyrolysis of Biomass: Advances in Science and Technology
Edited by Robert C. Brown and Kaige Wang
© The Royal Society of Chemistry, 2017
Published by the Royal Society of Chemistry, www.rsc.org

substantially between feedstock types. Furthermore, the commoditization of biomass feedstocks will likely result in the distribution of feedstock "blends", or combinations of several feedstock species (*e.g.* pine wood, switchgrass, and poplar wood), the proportions of which will typically be determined by economic factors such as harvesting, preparation, transportation costs, supply levels and market demand for the various constituents.

Ideally, biomass conversion processes should be robust to changing economic conditions and thereby able to maintain acceptable product yields and quality for a wide range of potential feedstocks. However, the inherent variability of biomass feedstocks presents significant process development challenges. This is especially true for thermochemical conversion processes such as fast pyrolysis, where feedstock variations can have a major impact on process performance and economics.

While feasibility studies of biomass fast pyrolysis typically focus on process simulations at the reactor scale, intra-particle processes can often become rate limiting. Thus particle-scale modeling has indeed received considerable attention from the scientific community in recent years. The vast majority of these studies have attempted to couple various kinetic models with highly simplified particle geometries along with estimates for the time and temperature histories experienced by individual biomass particles.[1–11] While these approaches can provide good agreement with the trends observed in specific experiments, their predictive utility is limited since feedstock-specific effects, such as variations of intra-particle transport due to species-specific characteristics, are typically lumped together with the intrinsic reaction kinetics in the form of rate parameters that do not resolve differences between structural and molecular effects.

Recent attempts to more effectively address the impact of biomass particle properties have included models that account for realistic particle shapes[12] as well as the anisotropic, intra-particle transport behavior that arises from the highly directional cellular structure.[13] These efforts have certainly advanced biomass particle modeling; yet recent experience indicates that the next generation of biomass conversion modeling will need to establish even more refined relationships between feedstock-dependent physical features, such as microstructure and composition, and particle-scale transport and chemical reaction parameters. Also, to be practically useful, pyrolysis simulation models should strive to minimize computational overhead, so that it is possible to make timely investigations of how reactor design and operating changes might be used to maintain yield and quality in spite of feedstock variations. Ultimately, this might include the possibility of implementing on-line model-based process control to continuously optimize process performance. As we discuss next, it appears to us that this type of model order reduction can be achieved for fast biomass pyrolysis by combining thoughtful use of suitable approximations for key transport and reaction processes with model verification by more detailed, complex simulations. Such reduced order models for particle-scale pyrolysis will facilitate efficient integration into reactor and process-scale simulations relevant to both research and industrial interests.

In this chapter, we summarize recent advances in biomass particle-scale modeling that are relevant to fast pyrolysis simulations. We begin by describing the physical structure of biomass particles and how that structure relates to intra-particle processes during fast pyrolysis. Next, we summarize the state of the art in characterizing and predicting the pyrolysis reaction chemistry and kinetic mechanisms that are driven by the rapid heating. Furthermore, we describe approaches for addressing transport effects with even simpler models and add reaction kinetics to produce simulations that predict product compositions and yields. Finally, we summarize our view of the current limitations and discuss opportunities that remain in the area of computational particle-scale modeling of biomass fast pyrolysis.

11.2 Overview of Biomass Structure

Plant-derived biomass is a porous, biopolymer composite material with a complex hierarchical structure. This structure is inherited from the remains of once-living plant tissue, where the anatomy of the original plant organism is manifested at every length scale.[14] At the macroscale, inter-species differences such as branching patterns in trees, or stem thicknesses and internode distances in grasses, are visually obvious. At the microscale, the dominant structural feature of biomass is imparted by the cellular arrangement of the tissue. Many of these features are visually depicted in Figure 11.1 for coniferous softwood, which is a common type of feedstock for biomass fast pyrolysis. Due to the tiered structure of biomass, computational simulation of any type of thermochemical biomass conversion requires an inherently multiscale approach.

A scanning electron micrograph (SEM) showing the microstructure of yellow pine is shown in Figure 11.1c. During the life of the organism, the primary function of the tissue is to transport water and nutrients throughout the plant, giving rise to many high-aspect-ratio cells oriented parallel to the trunk or stem which strongly influences the density and thermal properties of the wood. Furthermore, transport of molecular species liberated during pyrolysis processes occurs *via* convection within these open cell lumen, which is much faster than intra-cell wall transport which is primarily limited to diffusion.

Secondary cell walls, such as that of yellow pine depicted by the transmission electron micrograph (TEM) shown in Figure 11.1d, account for the majority of the mass in wood and grasses. The biopolymer composition of these different regions is known to vary significantly; the lignin composition is typically higher in the compound middle lamella (abbreviated CML, the region between adjacent cells) than in the secondary cell wall (SCW). The impact of these different regions on thermochemical conversion processes is not entirely understood at present; however, it has been recently shown that intra-cell wall diffusion for some molecules, particularly ions, is a strong function of local moisture content and occurs at different rates through the CML than the SCW.[15] These observations suggest that the local biopolymer

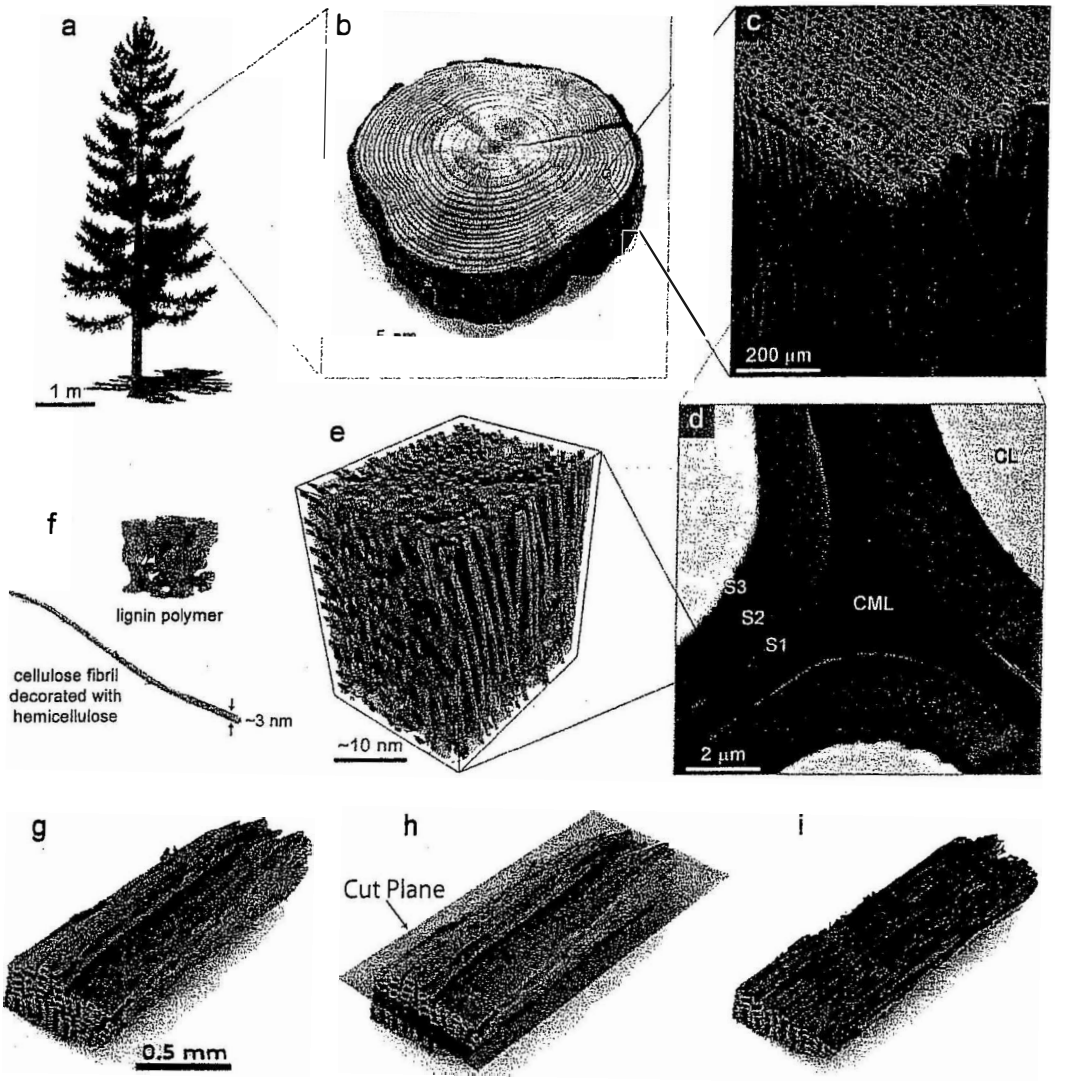

Figure 11.1 Multiscale visualization of wood structure and a typical woody feedstock. (a) Depiction of a coniferous tree. (b) Optical micrograph of section of a pine trunk. (c) Scanning electron micrograph of wood tissue showing cellular structure. (d) Transmission electron micrograph of cell wall showing various layers of the cell wall. CML: compound middle lamella; CL: cell lumen; S1, S2, and S3 denote layers of the secondary cell wall. (e) Depiction of the nanoscale arrangement of biopolymers within the cell wall. (f) Depiction of amorphous lignin polymer and a cellulose fibril decorated with hemicellulose. (g–i) X-Ray computed tomography reconstruction of a milled pine particle. The cutaway image reveals intact, directional porosity contributed by the cellular structure. Figure panels a–f reprinted with permission from ref. 14. Copyright 2016 American Chemical Society. Data in figure panels g–i are unpublished, courtesy of Joseph Jakes, USDA Forest Products Lab.

composition, which varies substantially between species and even between tissue types of the same species (particularly in grasses), can impact rates of intra-cell wall molecular transport which in turn impacts the intra-particle residence time of products formed during fast pyrolysis.

A depiction of the arrangement of nanoscale biopolymers within a secondary cell wall is shown in Figure 11.1e. Unlike conventional synthetic polymer assemblies, the nanostructure of biomass is highly ordered. Excellent, detailed discussions of the synthesis, molecular structure, and arrangement of these biopolymers are available in the literature.[16,17] In brief, cellulose nanofibrils provide the scaffolding of the cell wall; hemicellulose acts to crosslink the cellulose; and lignin, a generally amorphous polymer that imparts hydrophobicity, provides structural support, and microbial defense to the cell wall matrix. During pyrolysis, these macromolecules are thermally depolymerized to smaller, volatile compounds that must exit the remains of the cell wall and the particle.

Fast pyrolysis, like most thermochemical conversion processes, requires some form of preliminary size reduction of the raw harvested biomass. This initial step inevitably results in a range of feed particle sizes and shapes, depending on both the mechanical action of the milling process as well as the original properties of the biomass.[18] Both the size[19] and shape[12] of the reduced biomass particles can subsequently impact fast pyrolysis performance by affecting the rates of heat and mass transfer that drive the intra-particle decomposition reactions. X-ray computed tomography (XCT) reconstructions of a milled pine particle as shown in Figure 11.1g–i exemplify the non-spherical geometry that is typical of milled biomass particles. The cutaway image shown in Figure 11.1h illustrates that the internal, highly directional porosity is preserved through the milling process. All of these structural features impact the outcome of fast pyrolysis; thus the challenge of building realistic particle models with enhanced utility lies in the accurate, quantitative measurement of these structural features and subsequently incorporating them into simulations.

11.3 Representing the Microstructure, Morphology, and Material Properties of Biomass in Particle Models

Capturing the complexity of biological structures and systems *in silico* is indeed challenging in general, and biomass particles are no exception. As with most computational undertakings, increasing degrees of complexity and detail provides improved accuracy and reliability but comes at the expense of increased computational resources such as longer compute times and memory requirements. The complexity of the problem is depicted in Figure 11.2 with structural models of woody biomass particles. Various imaging techniques such as XCT and SEM provide detailed structural information that can be used to quantify key geometric features. In the case of XCT, the

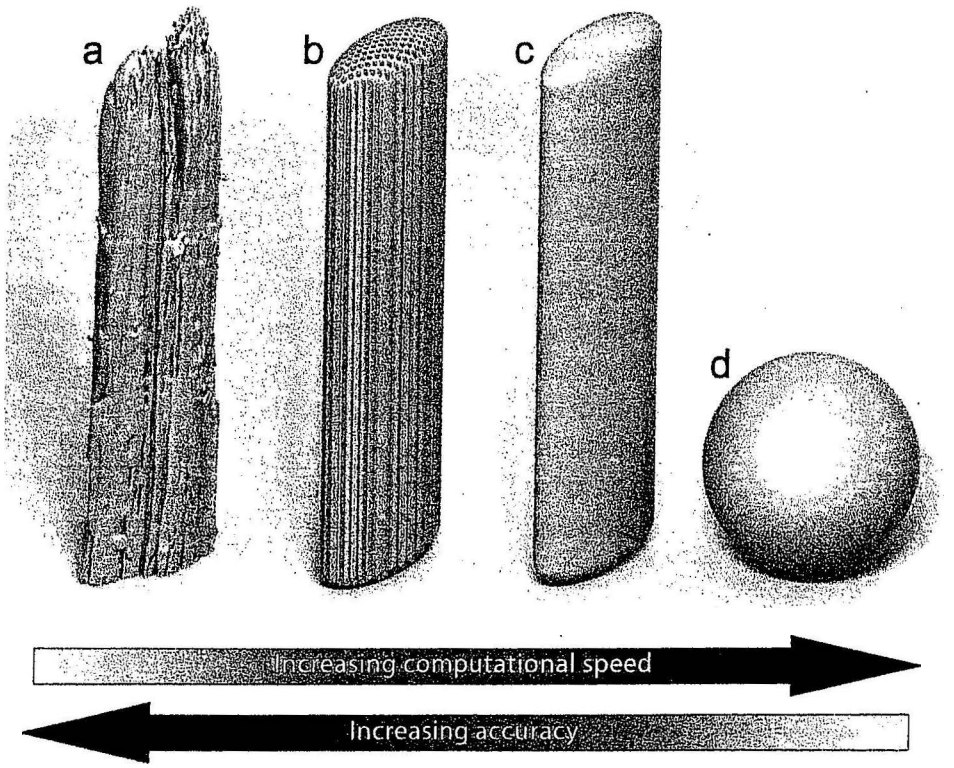

Figure 11.2 Prediction accuracy for particle models increases as more geometric details are included at the expense of reduced computational speed. (a) Full XCT model of actual wood particle. (b) Simplified geometry accounting for surface features and internal microstructure. (c) Basic geometry representing bulk surface area and volume of realistic wood particle. (d) Spherical representation of a biomass particle.

irregular geometry of actual biomass particles may be directly "mapped" into a 3-D computer modeling environment.[20] With a voxel size of ~0.5 μm, this technique provides excellent spatial resolution for resolving the microstructure of biomass and can be used to produce isosurface 3-D representations suitable for importing into computational environments such as finite element simulation software. An example of such a model is presented in Figure 11.2a. The drawback of such highly resolved particle representations is that the resulting computational analysis requires a massive number of finite elements for a particle of just a few millimeters in length. Thus for the level of detail in Figure 11.2a, computational simulations of pyrolyzing biomass particles become extremely expensive, and possibly prohibitively so, even for current high-performance computing systems. We speculate that such simulations will become more tractable as computing hardware and software continue to evolve, but no such detailed simulations based on direct XCT reconstructions have been reported to date for biomass fast pyrolysis.

Recently, we proposed an alternative method for the construction of 3-D biomass particle models that explicitly captures major structural features of the particle, such as the overall size and morphology of the particle and the

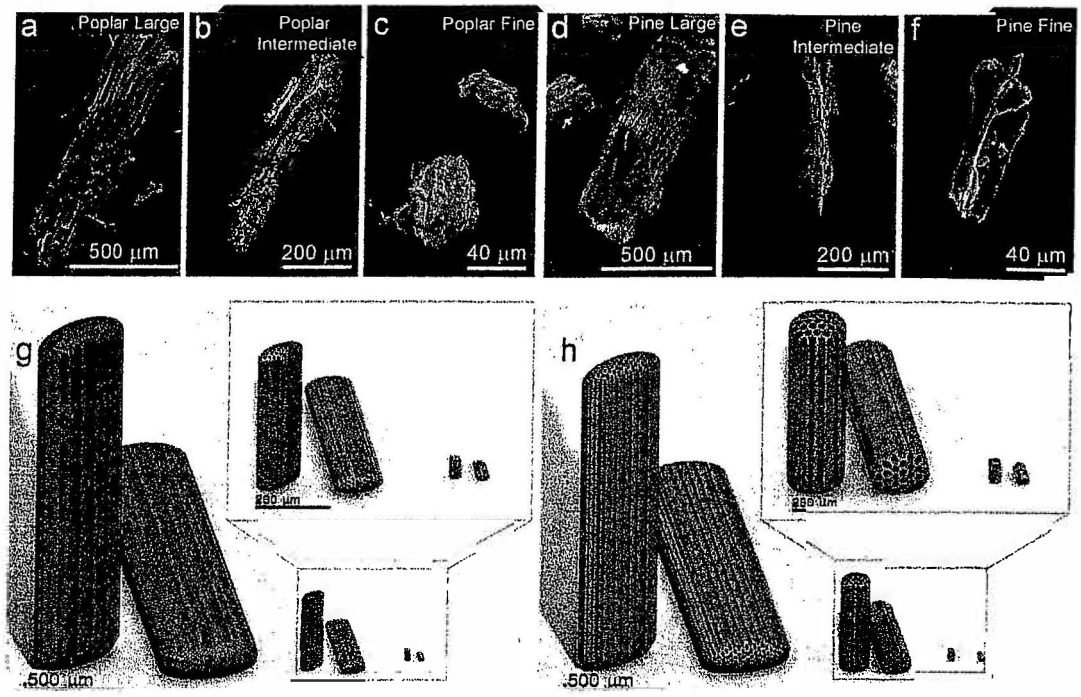

Figure 11.3 SEM and microstructure particle models of hardwood and softwood. SEM images showing representative poplar (a–c) and pine (d–f) particles. (g,h) Orthographic visualization of particle models constructed by the CSG algorithm using the dimensions and morphological parameters measured from image analysis. Inset panels show a zoom view of the intermediate and fine size classes of each feedstock. Reprinted with permission from ref. 21. Copyright 2015 American Chemical Society.

internal porosity due to the axially aligned fiber cells and vessel elements.[21] An example of one such particle model is presented in Figure 11.2b. This approach employs multiscale imaging coupled to quantitative image analysis to extract structural parameters such as the external particle size and shape from images of milled feedstock; as well as the average cell wall thickness and lumen diameters of axial tracheids and vessel elements from confocal scanning laser micrographs of particle cross-sections. These parameters are used in a custom constructive solid geometry (CSG) algorithm to build a 3-D particle model that serves as a representative surrogate of the morphological features obtained from the image analysis.

Examples of these surrogate models at various particle sizes constructed by CSG for milled pine and poplar feedstocks are presented in the lower portion of Figure 11.3. This figure demonstrates how CSG can be used to construct particle representations that account for size and shape variations along with internal features such as cell walls and axially oriented lumen. These particle models involve some loss of detailed morphological information, but the simplified structure facilitates more efficient finite element simulations of particles using present-day high-performance computing resources.

11.4 Simulating Intra-Particle Transport Phenomena

The complex internal structure of biomass provides a framework in which multiple transport processes occur during fast pyrolysis. It has been recognized that maximizing particle heating rate is critical to achieve high-yields of bio-oil.[22] Ideally, both heat transfer from the reactor environment to the biomass particles as well as intra-particle heat transfer should be as fast as possible. Because pyrolysis releases vapors and viscous liquids, heat transfer within the particle cell lumen is accompanied by fluid convection. Similarly, diffusive and convective mass transfer processes play important roles in pyrolysis as the thermal degradation products exit the particle. All these physical processes are strongly coupled to chemical reactions that produce both desired and undesired products.

11.4.1 Governing Equations for Transport

In the most general case, simulation of the intra-particle transport processes during biomass fast pyrolysis requires solving three-dimensional partial differential conservation equations for energy, mass, and momentum. If we temporarily ignore the generation terms associated with chemical reactions, the governing equations can be summarized mathematically by a series of coupled, partial differential equations (PDEs):

$$\frac{\partial \rho}{\partial t} + \nabla\cdot(\rho \mathbf{u}) = 0 \tag{11.1}$$

$$\rho\frac{\partial \mathbf{u}}{\partial t} + \rho\mathbf{u}\cdot\nabla\mathbf{u} = -\nabla p + \nabla\cdot\left[\mu\left(\nabla\mathbf{u} + (\nabla\mathbf{u})^T\right) - \frac{2}{3}\mu(\nabla\cdot\mathbf{u})\mathbf{I}\right] \tag{11.2}$$

$$\rho C_p\left(\frac{\partial T}{\partial t} + (\mathbf{u}\cdot\nabla)T\right) = \nabla\cdot(k\nabla T) \tag{11.3}$$

where ρ is the fluid density, $\mathbf{u}$ is the velocity vector, p is the pressure, μ is the viscosity, $\mathbf{I}$ is the identity matrix, and T is the temperature (superscript T denotes the transpose operator in eqn (11.2)). In the solid domain of the biomass particle (*i.e.* within the cell walls, but not within the cell lumen), the convective component of the heat equation, $(\mathbf{u}\cdot\nabla)T$, may be omitted based on the assumption that the particle remains solid and conduction is the dominant mode of heat transfer. However, it has been demonstrated that biomass particles undergo a molten-phase transition en route to vaporization in many cases.[23] In such cases modeling the biomass particle as an extremely viscous liquid with local, temperature dependent viscosity may be more appropriate.

Pyrolyzing biomass particles that are large enough to exhibit significant spatial thermal gradients contain distinctive zones as they convert from virgin biomass to char and pyrolysis vapors within the lumens. Vapors present within the particle contain multiple components including the inert gas serving as the reactor media (typically nitrogen), condensable vapor-phase

products of pyrolysis, and non-condensable light gases. In many cases, the dynamic, localized variations in the material properties can be approximated by the general rule of mixtures,[24] wherein local properties are calculated as the weighted mean of n individual components as

$$\theta_E = \sum_i^n f_i \theta_i \tag{11.4}$$

where θ_E is the ensemble material property (*e.g.* density, thermal conductivity, heat capacity, *etc.*), θ_i is the specific material property of the ith component of the ensemble, and f_i is the volume fraction of the ith material given by

$$f_i = \frac{V_i}{V_E} = \frac{V_i}{\sum_i^n V_i} \tag{11.5}$$

In the case of finite element simulations employing this strategy, all relevant material properties are evaluated by eqn (11.5) within each volume element at each time step. Because these properties are often strong functions of temperature and degree of conversion, the resulting system of PDEs can become highly non-linear, which often necessitates very small time steps, and subsequently long compute times, to achieve convergence.

Several strategies exist for solving the above transport equations computationally, the choice of which depends primarily upon the level of geometric complexity considered. Finite element methods (FEMs), which are discussed below, are typically required to simulate the most geometrically complex particle models, while less sophisticated PDE or ordinary differential equation (ODE) solvers are suitable for evaluating models with simplified geometry or reduced dimensionality. Regardless of the computational methods used, the utility of single particle simulations can be greatly enhanced by performing ensemble calculations to model the behavior of real feedstocks that contain a distribution of particle sizes, shapes, and biomass species.

11.4.2 Finite Element Simulations

Since the FEM has the ability to represent virtually any type of complex particle geometry, simulation results generated by this method are especially good for resolving the impact of detailed morphological complexity on transport processes. For this reason, FEM also provides a reliable point of reference for assessing the accuracy of less spatially resolved models. FEM subdivides the simulation geometry into smaller domains, or elements, over which boundary-value PDEs are solved. A detailed discussion of the mathematical fundamentals of this approach is outside the scope of this chapter; however, the interested reader is pointed to several excellent texts on the topic.[25,26]

As mentioned above, the geometry of biomass particles often departs significantly from simple shapes such as spheres or cylinders and contains highly variable internal porosity. Many types of biomass particles contain pores with diameters ranging from 50–100 μm (*e.g.* vessel elements in hardwoods and

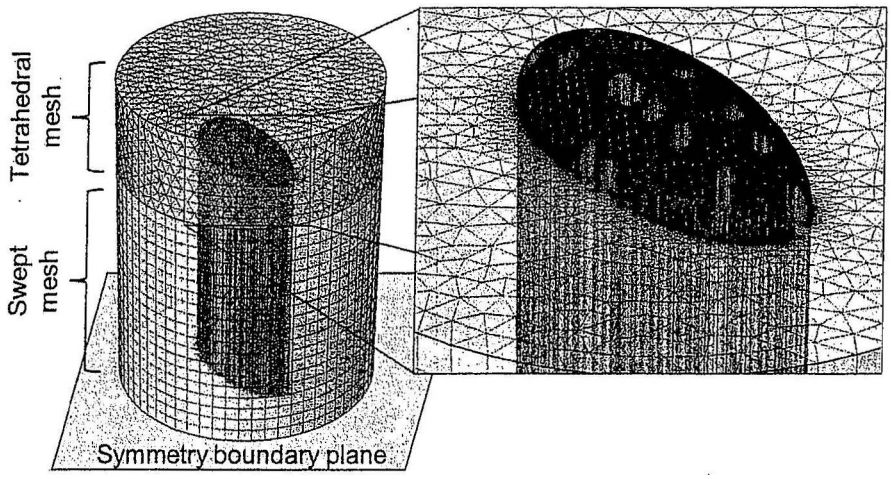

Figure 11.4 Finite element mesh and symmetry plane of a 2 mm aspen particle. Symmetry and variable mesh sizes can be utilized to reduce simulation time. Reprinted with permission from ref. 21. Copyright 2015 American Chemical Society.

vascular tissue in grasses), which can be on the same order of the dimensions of the particle exterior especially for high-aspect-ratio particles. Therefore, FEM affords the ability to explicitly account for not only the external morphology of biomass particles but also their internal porosity when necessary. However, the primary drawback to this method is the large computational expense associated with simulating geometries that require a large number of elements.

Figure 11.4 illustrates an example mesh used for FEM simulations of a ~2 mm aspen particle model which explicitly accounts for the distribution of vessel cells and axial tracheids within the particle. Even after applying applicable symmetry planes and meshing techniques such as swept prismatic meshing to reduce the number of elements, a suitable mesh for this geometry still requires ~4.8 million elements. In FEM simulations, the number of degrees of freedom that must be solved numerically scale roughly as the product of the number of elements and the number of dependent variables, which can make simulations of the geometry shown in Figure 11.4 extremely memory intensive and require long compute times even when solving for just a few dependent variables. Advances in computing hardware and solver methods such as domain decomposition will undoubtedly facilitate increasingly larger simulations in the future; however, in some cases suitable low-order approximations can be employed. Considering the constraints of current computing capabilities, the use of such high-resolution FEM models is probably most useful for identifying how and when low-order approximations are applicable to facilitate efficient use of computational resources.

11.5 Simulating Particle-Scale Reactions

Accurately predicting yields and compositions of the products from biomass fast pyrolysis also requires basic information about the rate at which chemical species are consumed and generated. Additional source

and sink terms are needed in the mass and energy equations to account for these reactions. As an initial step, it is important to recognize that the structural geometry of lignocellulosic biomass is typically formed from a complex matrix of polymers with monomers consisting of cellulose ($C_6H_{10}O_5$), hemicellulose ($C_5H_8O_4$), and lignin (primarily $C_{22}H_{28}O_9$, $C_{20}H_{22}O_{10}$, $C_{15}H_{14}O_4$).[27,28] The relative amounts of these different macromolecules vary significantly among different feedstock species. In addition, there are small amounts of lower molecular weight organic species, inorganic minerals, and water. The inorganic minerals make up the residual ash left after complete devolatilization. The water initially contained in the biomass feed particles can exist in three different states: bound water which is closely associated with the carbohydrate components of the cell wall, free liquid water which is present within the cell lumen, and vapor.

All of the above components can play significant roles in the reactions (which can potentially number in the hundreds or thousands) that occur during pyrolytic conversion. Taken together, explicit simulation of all the possible species and reactions during biomass fast pyrolysis is simply beyond the current state of the art and is likely to remain so for some time. However, significant progress has been made towards developing reduced reaction mechanisms that can at least make predictions about the rates of formation of lumped product classes such as light gases, char, and tar.[28–32] In most cases, the global kinetics for these reduced reaction mechanisms are represented with first-order Arrhenius expressions in which all temperature dependence is restricted to the exponential term:

$$K_i = A_i e^{-E_i/RT}$$
$$\frac{dC_i}{dt} = C_i K_i \tag{11.6}$$

where K is the rate constant (1 s^{-1}), A is the pre-factor (1 s^{-1}), E is the activatione energy (kJ mol^{-1}), R is the gas constant (kJ mol^{-1} K^{-1}), T is the temperaturee (Kelvin), and C is typically a mass-based concentration (kg m^{-3}) representinge gasetar, char, or wood. Table 11.1 summarizes examples of some of the simplest proposed mechanisms and their associated parameters available in the literature while Table 11.2 summarizes examples of more complex proposed mechanisms and their kinetic parameters.

An important shortcoming of the currently available reaction mechanisms and kinetics is that many of these produce inconsistent predictions, even for the same reaction conditions. This is illustrated in Figure 11.5, which depicts the fractional wood conversion and tar yield *versus* time predicted by several of the kinetic schemes in Tables 11.1 and 11.2 assuming a constant temperature of 500 °C (773 K). We conjecture that a significant portion of the disagreement between these different schemes may be the result of undocumented differences in the biomass used for experimental measurements as well as the inadvertent manifestation of feedstock species-specific transport effects in the fitted kinetic parameters.e

Table 11.1 Examples of simple primary and secondary reaction mechanisms and global kinetic parameters available in the current biomass pyrolysis literature. Pre-factor represented by A (1 s^{-1}) and activation energy by E (kJ mol^{-1}).

Reference	Kinetic scheme	Kinetic parameters
Di Blasi[31] Font[37] Thurner[38]	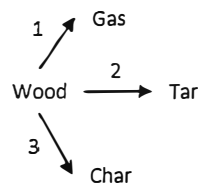	$A_1 = 1.4 \times 10^4$ to 4.4×10^9 $A_2 = 4.1 \times 10^6$ to 1.1×10^{10} $A_3 = 2.9 \times 10^2$ to 3.3×10^6 $E_1 = 88.6$ to 156 $E_2 = 112.7$ to 148 $E_3 = 61$ to 111.7
Di Blasi[39] Janse[40] Papadikis[41]	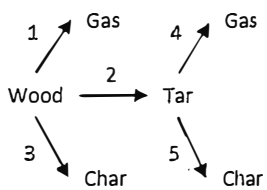	$A_1 = 5.2 \times 10^6$ to 1.1×10^{11} $A_2 = 2.0 \times 10^8$ to 1.5×10^{10} $A_3 = 1.1 \times 10^7$ to 2.7×10^{10} $A_4 = 8.6 \times 10^4$ to 4.3×10^6 $A_5 = 7.7 \times 10^4$ to 1.0×10^6 $E_1 = 88.6$ to 177 $E_2 = 112.7$ to 149 $E_3 = 106.5$ to 125 $E_4 = 87.8$ to 108 $E_5 = 87.8$ to 108
Koufopanos[42]		$A_1 = 9.97 \times 10^{-5}$ $G_1 = 17254.4$, $L_1 = -9061227$ $A_2 = 1.068 \times 10^{-3}$ $G_2 = 10224.4$, $L_2 = -6123081$ $A_3 = 5.7 \times 10^5$, $E_3 = 81$
Chan[43]	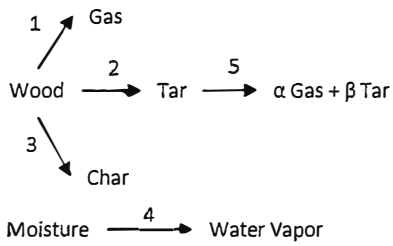	$A_1 = 1.3 \times 10^8$, $E_1 = 140$ $A_2 = 2.0 \times 10^8$, $E_2 = 133$ $A_3 = 1.08 \times 10^7$, $E_3 = 121$ $A_4 = 5.13 \times 10^6$, $E_4 = 87.9$ $A_5 = 1.48 \times 10^6$, $E_5 = 144$
Liden[44]	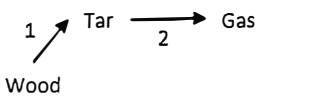	$A_2 = 4.28 \times 10^6$, $E_2 = 107.5$ $A = 1 \times 10^{13}$, $E = 183.3$ Where A and E is total wood conversion, reactions 1 and 3
Sadhukhan[45]	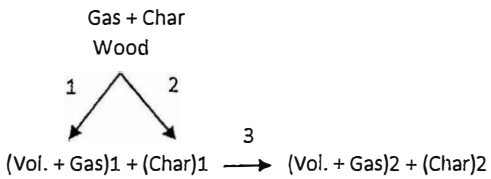	$A_1 = 168.4$, $E_1 = 51.965$ $A_2 = 13.2$, $E_2 = 45.96$ $A_3 = 5.7 \times 10^6$, $E_3 = 92.4$

Table 11.2 Examples of complex fast pyrolysis reaction mechanisms and their associated global kinetic parameters as proposed in the current literature. A is the pre-factor (1 s^{-1}) while E is the activation energy (kJ mol^{-1} for the Miller and Bellan and the Anca-Couce kinetic schemes and parameters, and kcal $kmol^{-1}$ for the Ranzi kinetic scheme and parameters).

Miller and Bellan kinetic scheme and parameters[32]

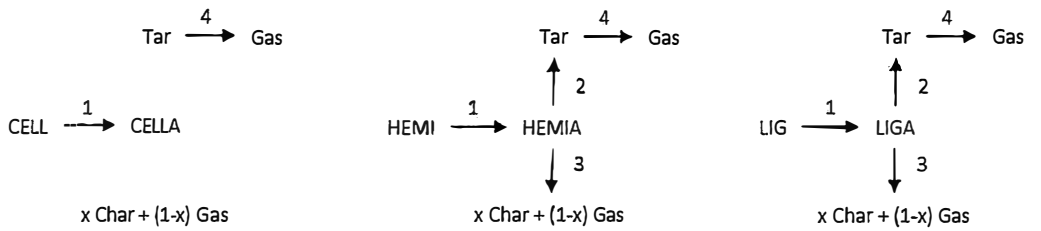

Cellulose	Hemicellulose	Lignin
$A_1 = 2.8 \times 10^{19}$, $E_1 = 242.4$	$A_1 = 2.1 \times 10^{16}$, $E_1 = 186.7$	$A_1 = 9.6 \times 10^{8}$, $E_1 = 107.6$
$A_2 = 3.28 \times 10^{14}$, $E_2 = 196.5$	$A_2 = 8.75 \times 10^{15}$, $E_2 = 202.4$	$A_2 = 1.5 \times 10^{9}$, $E_2 = 143.8$
$A_3 = 1.3 \times 10^{10}$, $E_3 = 150.5$	$A_3 = 2.6 \times 10^{11}$, $E_3 = 145.7$	$A_3 = 7.7 \times 10^{6}$, $E_3 = 111.4$
$A_4 = 4.28 \times 10^{6}$, $E_4 = 108$	$A_4 = 4.28 \times 10^{6}$, $E_4 = 108$	$A_4 = 4.28 \times 10^{6}$, $E_4 = 108$

Ranzi kinetic scheme and parameters[28]

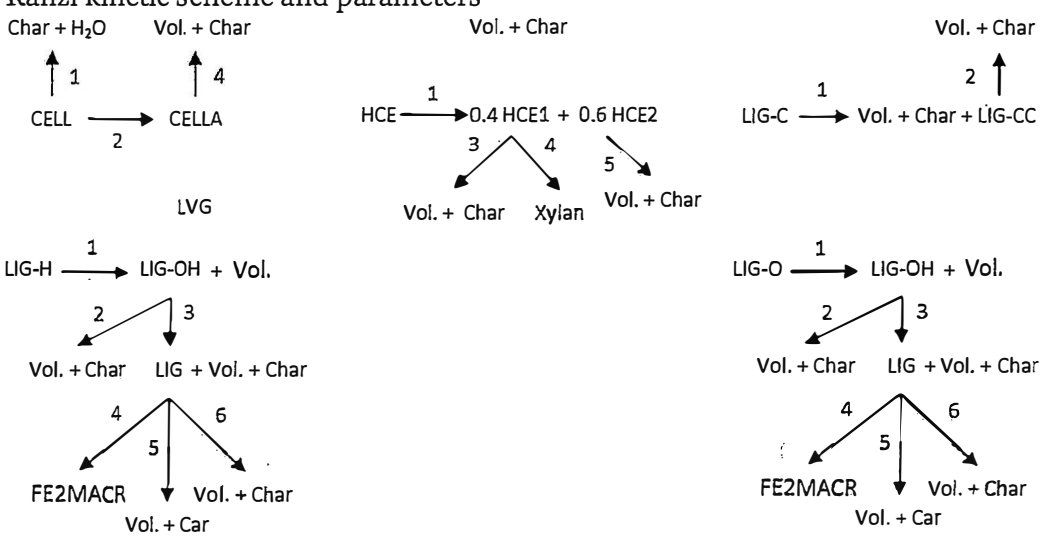

Cellulose	Hemicellulose	Lignin-C
$A_1 = 4.0 \times 10^{7}$, $E_1 = 31\,000$	$A_1 = 0.33 \times 10^{10}$, $E_1 = 31\,000$	$A_1 = 1.33 \times 10^{15}$, $E_1 = 48\,500$
$A_2 = 4.0 \times 10^{13}$, $E_2 = 45\,000$	$A_2 = 1.0 \times 10^{9}$, $E_2 = 32\,000$	$A_2 = 1.6 \times 10^{6}$, $E_2 = 31\,500$
$A_3 = 1.8 \times T$, $E_3 = 10\,000$	$A_3 = 0.05 \times T$, $E_3 = 8000$	
$A_4 = 0.5 \times 10^{9}$, $E_4 = 29\,000$	$A_4 = 0.9 \times T$, $E_4 = 11\,000$	
	$A_5 = 0.33 \times 10^{10}$, $E_5 = 33\,000$	

Lignin-H	Lignin-O
$A_1 = 0.67 \times 10^{13}$, $E_1 = 37\,500$	$A_1 = 0.33 \times 10^{9}$, $E_1 = 25\,500$
$A_2 = 33$, $E_2 = 15\,000$	$A_2 = 33$, $E_2 = 15\,000$
$A_3 = 0.5 \times 10^{8}$, $E_3 = 30\,000$	$A_3 = 0.5 \times 10^{8}$, $E_3 = 30\,000$
$A_4 = 2.4 \times T$, $E_4 = 12\,000$	$A_4 = 2.4 \times T$, $E_4 = 12\,000$
$A_5 = 0.4 \times 10^{9}$, $E_5 = 30\,000$	$A_5 = 0.4 \times 10^{9}$, $E_5 = 30\,000$
$A_6 = 0.083 \times T$, $E_6 = 8000$	$A_6 = 0.083 \times T$, $E_6 = 8000$

(*continued*)

Table 11.2 *(continued)*

Anca-Couce kinetic scheme and parameters[29]

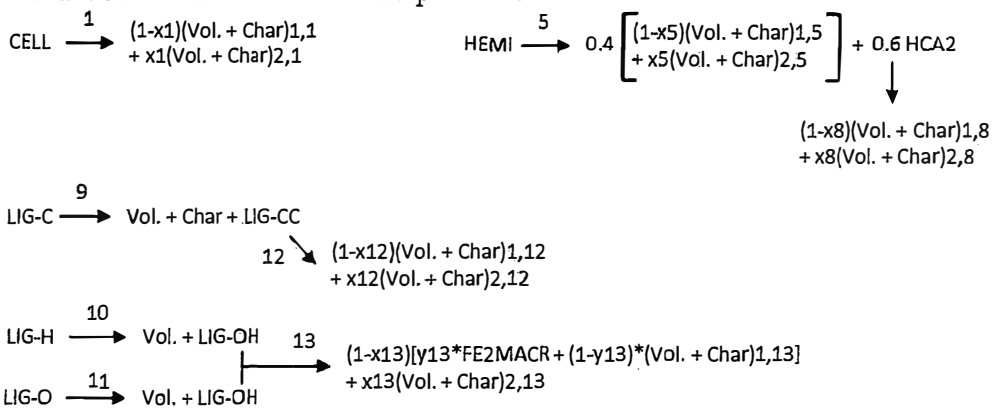

Cellulose $A_1 = 8 \times 10^{13}$, $E_1 = 192.5$	Hemicellulose $A_5 = 1 \times 10^{10}$, $E_5 = 129.7$ $A_8 = 1 \times 10^{10}$, $E_8 = 138.1$
Lignin-C $A_9 = 4 \times 10^{15}$, $E_9 = 202.9$ $A_{12} = 5 \times 10^{6}$, $E_{12} = 131.8$	Lignin-H and Lignin-O $A_{10} = 2 \times 10^{13}$, $E_{10} = 156.9$ $A_{11} = 1 \times 10^{9}$, $E_{11} = 106.7$ $A_{13} = 3 \times 10^{8}$, $E_{13} = 125.5$

Other important shortcomings of the currently available reaction mechanisms and kinetics in the literature are:

- There is scarce information on the catalytic effects of inorganic components such as ash (even though there is evidence that these effects can be large).[30,33–36]
- There are large inconsistencies in the experimental conditions used to obtain kinetic measurements.
- Very few mechanisms have been derived from reaction rate measurements that include product categories other than light gas, char, and tar for heating rates (500–1000 °C s^{-1}) relevant to fast pyrolysis of actual biomass.
- There are almost no mechanisms that explicitly include a role for initial particle moisture.
- There is an apparent lack of agreement on which molecular species should be included in the lumped product categories associated with "light gases", "char", and "tar".

Our review of the current pyrolysis kinetics literature reveals an imperative need to address the above shortcomings in order to develop a truly robust capability to predict product yields and compositions for industrially relevant biomass feedstocks. Otherwise, accurate simulations will only be possible for specific biomass feeds which have been previously characterized under similar experimental conditions. Even then, such simulations can probably only be expected to be interpolative rather than predictive.

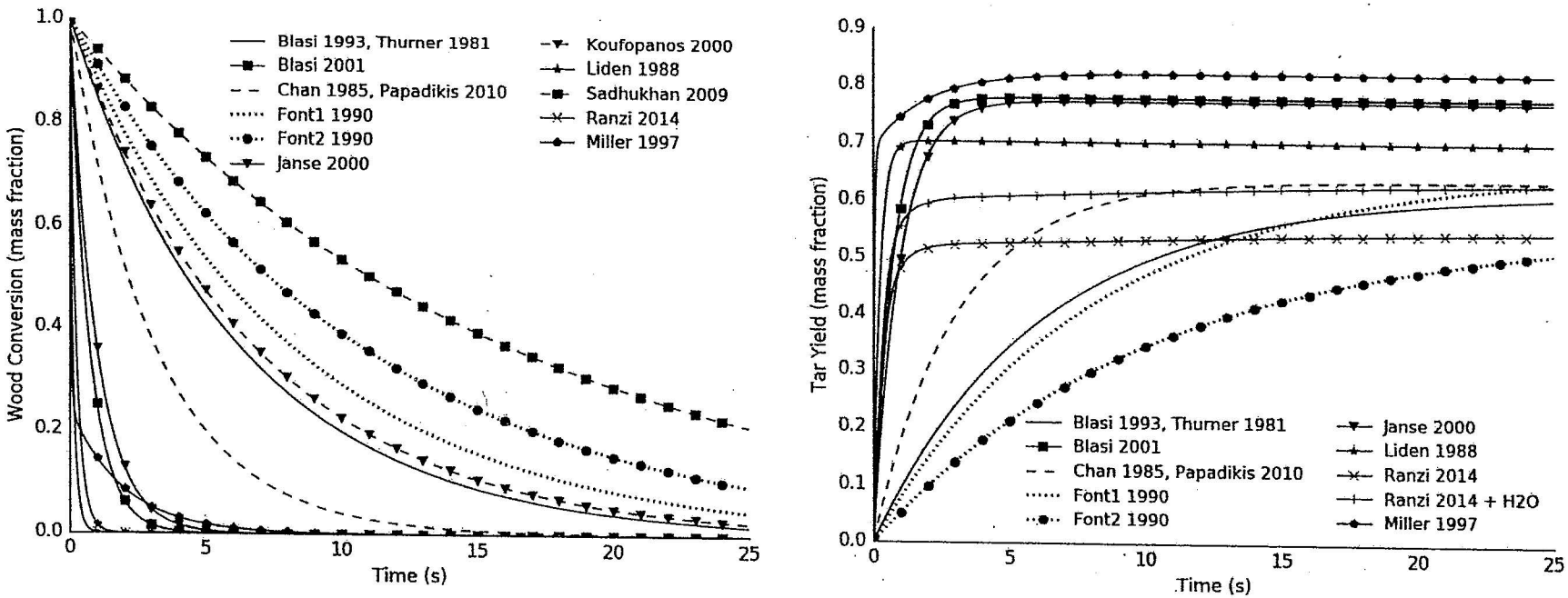

Figure 11.5 Comparison of predicted conversion and tar yield for wood pyrolyzed at 500 °C conditions based on selected kinetics from Tables 11.1 and 11.2. Left: fraction of the original wood remaining *versus* time. Right: primary tar yields *versus* time. Each line represents a particular scheme denoted by first author and year of publication.

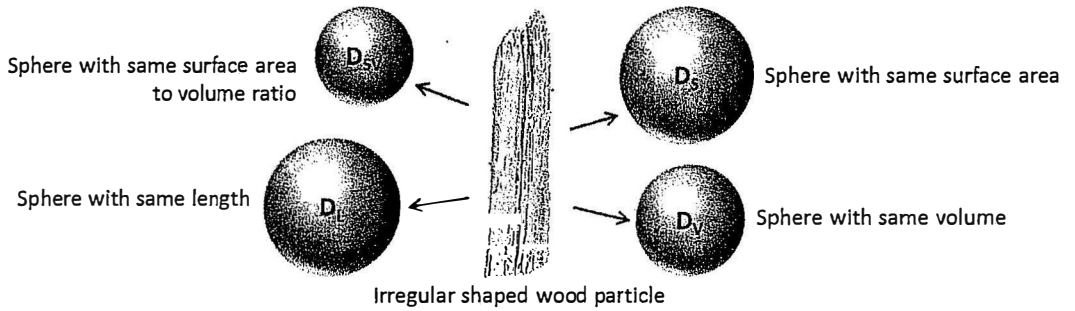

Figure 11.6 Equivalent spherical diameters to represent an irregularly shaped wood particle.

11.6 Approaches for Low-Order Particle Models

Even with the simplified 3-D geometry displayed in Figure 11.2c, it is extremely expensive to incorporate structural models with this level of detail into computational reactor-scale simulations involving thousands of biomass particles. Consequently, there is considerable motivation to develop lower-order modeling approaches that can account for the dominant particle-scale heat and mass transport effects involved in fast pyrolysis of biomass. One such approach is to approximate the multi-dimensional transport processes of biomass particles with idealized spherical particles having mathematically "similar" transport properties during rapid heat-up.[46] Figure 11.6 illustrates this concept for an irregularly shaped wood particle. We summarize an approach for utilizing this type of 1-D approximation in the following sections.

11.6.1 1-D Heat Transfer Approximations

Mathematically, approximations of 3-D transport processes are possible in 2-D and 1-D when a limited number of controlling parameters dominate the system and effectively reduce the dynamic phase space. In a recent study of particle-scale heat conduction under fast pyrolysis conditions, we demonstrated that this is typically the case for a realistic range of biomass particle sizes if the characteristic length used for 1-D simulations is based on the diameter of a surrogate spherical particle with a surface area to volume ratio (Dsv) equal to that of the original particle.[46] The significance of Dsv seems to confirm that the effective surface interface between each pyrolyzing particle and its surroundings is perhaps the most critical geometric factor controlling particle heat-up.

A widely used approach for simulating 1-D heat conduction in solid slab, cylindrical, and spherical geometries is based on solving the following transient PDE:[47]

$$\frac{1}{r^b}\frac{\partial}{\partial r}\left(kr^b\frac{\partial T}{\partial r}\right) = \rho C_p\frac{\partial T}{\partial t} \tag{11.7}$$

where r is the 1-D spatial coordinate (m), b is the shape factor (0 slab, 1 cylinder, 2 sphere), T is temperature in Kelvin (K), k is thermal conductivity ($W\,m^{-1}\,K^{-1}$), ρ is density ($kg\,m^{-3}$), C_p is heat capacity ($kJ\,kg^{-1}\,K^{-1}$), and t represents time in seconds(s). For particles with any of these shapes, spatial symmetry allows the application of a zero gradient at the particle center. The other relevant boundary condition for fast pyrolysis is the assumption that the heat flux at the particle surface can be represented by a convective heat transfer coefficient that accounts for the heat input through the external boundary layer.

As demonstrated in our particle modeling study,[46] eqn (11.7) can be successfully utilized with surrogate representations of typical biomass particles that assume a diameter (Dsv) that yields an equivalent surface area to volume ratio as the original particle. The results reported in the reference study also demonstrate that it is possible to use the bulk average thermal conductivity (k) and heat capacity (C_p) reported in standard references such as the Wood Handbook[48] for simulations. Although these bulk properties do not explicitly account for anisotropy, they effectively average the impact of the actual spatial variations. When combined with a surrogate 1-D representation of biomass particles, they appear to reasonably replicate the transient surface, center, and volume-average temperature profiles produced by the fully 3-D conductive heat transport as illustrated in Figure 11.7 for a loblolly pine particle exposed to conditions typical of fast pyrolysis.[46]

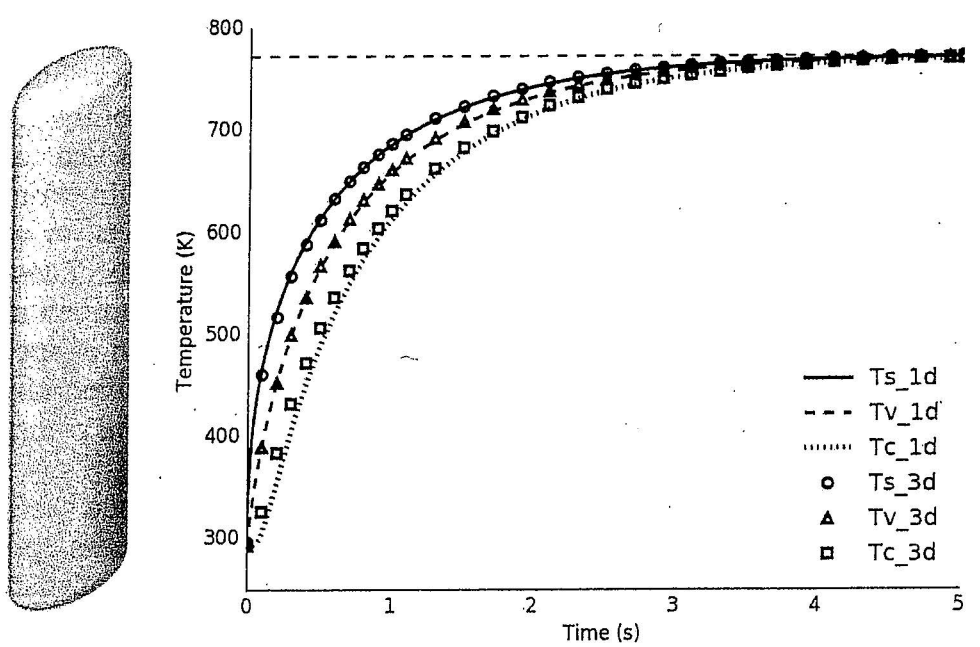

Figure 11.7 Comparison of temperature profiles from 3-D and 1-D model results for a loblolly pine particle at 500 °C (773 K). Bulk average properties of ρ = 540 kg m^{-3}, k = 0.12 W m^{-1} K^{-1}, and C_p = 103.1 + 3.867T J kg^{-1} K^{-1} provided by the Wood Handbook.[48] Particle surface area to volume diameter (Dsv) for one-dimensional model based on three-dimensional particle with a Feret diameter of 5.4 mm. Reprinted with permission from ref. 46. Copyright 2016 American Chemical Society.

11.6.2 Combining 1-D Heat Transfer and Reaction

In fast pyrolysis units, the amount of time it takes for a biomass particle to fully devolatilize is a critical parameter for reactor operation. In order to estimate this conversion, the 1-D model mentioned earlier can be coupled to a kinetic scheme to estimate pyrolysis yields and solid conversion time from wood to char. An example of combining the 1-D particle model to the kinetic scheme of Sadhukhan *et al.*[45] is shown in Figure 11.8. When the heat of reaction is included in the model the center temperature and conversion profiles match well with the experimental data for a 20 × 100 mm cylindrical wood particle. The temperature overshoot reported by the experiment at the center of the particle is also captured well with the 1-D model due to the exothermic heat of reaction. Without the heat of reaction, conversion time is prolonged and the temperature overshoot is not accounted for in the particle model. Since the model results do not account for mass transport within the particle, the effects of mass diffusion are assumed to be included to some extent *via* kinetic parameters of the reaction scheme.

11.7 Current Limitations in Particle-Scale Modeling

The recent the particle modeling efforts described above have made significant progress towards effectively capturing the complex and highly variable geometry of realistic biomass feedstocks; however, we feel that the absence of transport-independent conversion kinetics for biomass fast pyrolysis from the literature is presently the largest impediment to the development of a generalized pyrolysis model with accurate predictive capability across biomass feedstocks. In addition, more attention should be devoted to the incorporation of the catalytic effects of the ash content within biomass into kinetic schemes to accurately predict the pyrolysis products. In order to facilitate optimization of fast pyrolysis processes for the yields of desired chemical products, kinetic schemes must migrate away from lumped models and incorporate additional speciation to track the formation of specific molecules of interest. The implementation of these more detailed kinetic schemes will also require the use of reduced order models to be computationally feasible with present-day computational resources.

Additional improvements must also be made at the interface between particle modeling and reactor-scale modeling to facilitate process optimization and scale-up. Drag models have a large impact on the hydrodynamics predicted by CFD simulation software, but these models are typically established for spherical geometries which are not representative of biomass particles produced from milling and grinding processes. Improved drag models that are specific to biomass particles should be developed by combined experimental and computational efforts. These models must also be able to account for the distribution of particle shapes and sizes in order to predict particle behavior in realistic industrial scale fast pyrolysis processes. Similarly, interfacial heat transfer coefficients that

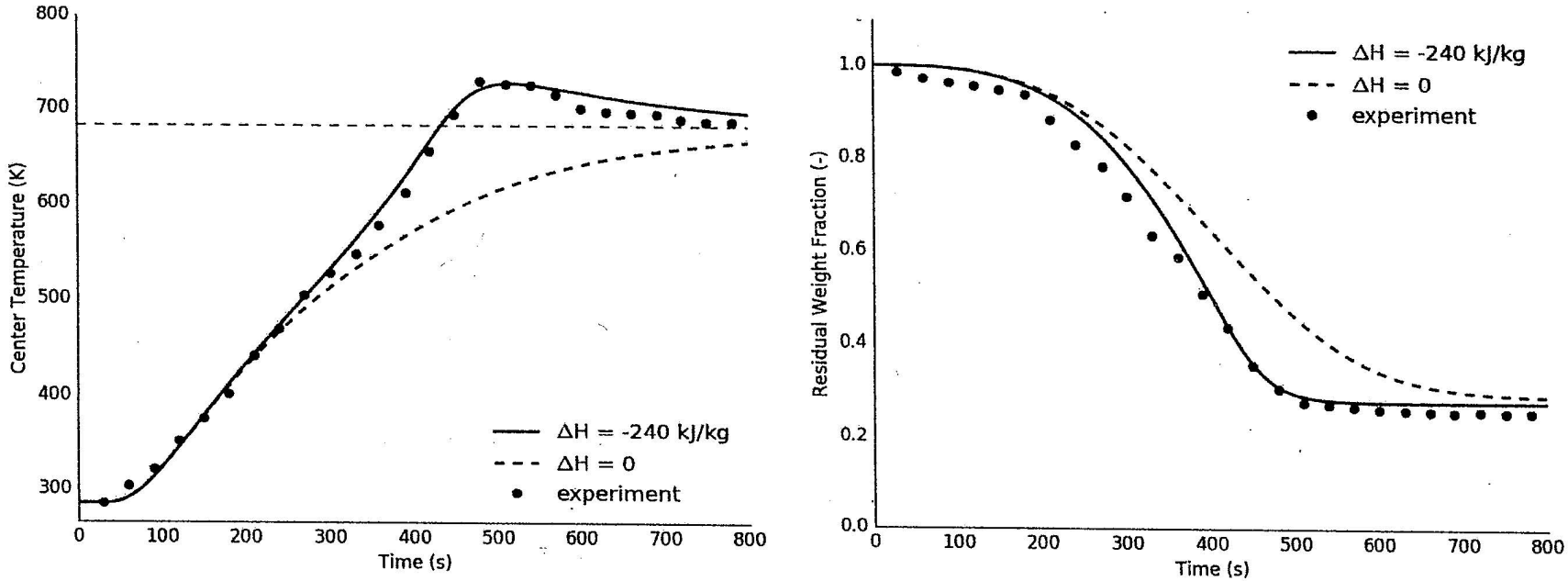

Figure 11.8 Center temperature profiles and conversion for a 20 × 100 mm wood cylinder at 683 K. Symbols represent experimental data from Sadhukhan *et al.*[45] The solid line denotes 1-D model results with $\Delta H = -240$ kJ kg^{-1} while the dashed line is with no heat of reaction. Reprinted with permission from ref. 46. Copyright 2016 American Chemical Society.

are typically used to model heat transfer from the reactor environment to the particle were developed for spherical particles. Our recent experience modeling interfacial heat transfer with realistic biomass particle models indicate that most correlations for heat transfer coefficients in the literature can provide poor agreement between simulations of conjugate heat transfer and simulations that employ interfacial heat transfer coefficients. Furthermore, we have observed interfacial heat transfer to be species-specific due to differences in particle microstructure that acts to modify the exterior geometry of the particle, and these species-specific affects are completely absent from the correlations in the current literature. In general, to accurately simulate the hydrodynamics and heating behavior of realistic biomass particles in pyrolysis reactors, many engineering correlations previously developed for other systems, such as coal pyrolysis, would need to be revisited in the context of realistic, species-specific biomass particle models.

11.8 Conclusions

Modeling fast pyrolysis at the particle scale provides the opportunity to assess the impacts of feedstock-specific parameters such as morphology, microstructure, composition, and moisture content. Since these parameters vary substantially between feedstocks, we feel that biomass particle modeling will be of increasing importance as we strive towards a renewable bioeconomy that commoditizes feedstocks and their biofuel and biochemical products provided by fast pyrolysis.

While the complexity of typical biomass feeds makes detailed computer simulations of individual particle behavior during fast pyrolysis extremely challenging, it is possible to develop 3-D representations of biomass particles that include the most important structural features revealed by advanced characterization methods such as XCT and SEM. FEM simulations using these 3-D representations can reveal important details of particle-scale processes during fast pyrolysis, but this comes at a high computational cost and thus must be used selectively. It is not currently feasible to use particle models with this level of structural detail in reactor simulations involving hundreds or thousands of particles.

Although numerous reaction mechanisms and kinetic parameters have been proposed for biomass fast pyrolysis, it appears that there remain serious shortcomings which need to be addressed. Chief among these are a lack of accounting for catalytic ash effects, inadequate separation of transport effects from intrinsic kinetics, inconsistent and poorly documented experimental protocols, inadequate differentiation of product species and associated reactions, and inadequate accounting for initial particle moisture. Until these shortcomings are resolved in the literature, we expect that it will not be possible to develop a truly robust predictive capability for an industrially relevant range of biomass feedstocks and feedstock blends.

1-D surrogate models of intra-particle conductive heat transfer can generate predictions of the transient intra-particle temperatures that are reasonable approximations of the simulation results produced by fully 3-D FEM simulations. The external surface area to volume ratio of particles is a key geometric factor, since it determines the available area per unit mass through which heat can enter the particle. Predictions from 1-D particle models combined with simplified pyrolysis kinetics generate predicted yields of char, light gas, and tar that appear to be reasonably consistent with experimental measurements. As with any modeling effort, the development of these improved models must be closely integrated with experimental results.

Overcoming the challenges described in this chapter will provide substantial benefit to the fast pyrolysis and biofuels community by enabling accurate predictions of feedstock-specific yields and optimal process conditions. This information will improve the state of technology and de-risk its commercialization, but development of these improved models will require large, coordinated efforts of computational and experimental teams.

References

1. B. V. Babu and A. S. Chaurasia, *Energy Convers. Manage.*, 2003, **44**, 2251–2275.
2. B. V. Babu and A. S. Chaurasia, *Energy Convers. Manage.*, 2004, **45**, 1297–1327.
3. C. Diblasi, *Combust. Sci. Technol.*, 1993, **90**, 315–340.
4. M. G. Gronli and M. C. Melaaen, *Energy Fuels*, 2000, **14**, 791–800.
5. A. M. C. Janse, R. W. J. Westerhout and W. Prins, *Chem. Eng. Process.*, 2000, **39**, 239–252.
6. C. A. Koufopanos, N. Papayannakos, G. Maschio and A. Lucchesi, *Can. J. Chem. Eng.*, 1991, **69**, 907–915.
7. K. Papadikis, S. Gu and A. V. Bridgwater, *Fuel Process. Technol.*, 2010, **91**, 68–79.
8. A. K. Sadhukhan, P. Gupta and R. K. Saha, *Bioresour. Technol.*, 2009, **100**, 3134–3139.
9. B. V. Babu and A. S. Chaurasia, *Chem. Eng. Sci.*, 2004, **59**, 1999–2012.
10. K. Papadikis, S. Gu and A. V. Bridgwater, *Chem. Eng. J.*, 2009, **149**, 417–427.
11. A. S. Chaurasia and B. D. Kulkarni, *Energy Convers. Manage.*, 2007, **48**, 836–849.
12. Y. Habibi, L. A. Lucia and O. J. Rojas, *Chem. Rev.*, 2010, **110**, 3479–3500.
13. C. DiBlasi, *Chem. Eng. Sci.*, 1996, **51**, 1121–1132.
14. H. Zhu, W. Luo, P. N. Ciesielski, Z. Fang, J. Zhu, G. Henriksson, M. E. Himmel and L. Hu, *Chem. Rev.*, 2016, **116**, 9305–9374.
15. S. L. Zelinka, S.-C. Gleber, S. Vogt, G. M. Rodríguez López and J. E. Jakes, *Holzforschung*, 2015, **69**, 441–448.
16. D. J. Cosgrove, *Nat. Rev. Mol. Cell Biol.*, 2005, **6**, 850–861.
17. J. H. Grabber, *Crop Sci.*, 2005, **45**, 820–831.

18. M. E. Himmel, M. Tucker, J. Baker, C. Rivard, K. Oh and K. Grohmann, *Biotechnology and Bioengineering Symposiom No. 15*, 1985, pp. 39–58.
19. J. Shen, X.-S. Wang, M. Garcia-Perez, D. Mourant, M. J. Rhodes and C.-Z. Li, *Fuel*, 2009, **88**, 1810–1817.
20. A. Isaac, V. Barboza, F. I. Sket, J. R. M. D'Almeida, L. A. Montoro, A. Hilger and I. Manke, *Biotechnol. Biofuels*, 2015, **8**, 1.
21. P. N. Ciesielski, M. F. Crowley, M. R. Nimlos, A. W. Sanders, G. M. Wiggins, D. Robichaud, B. S. Donohoe and T. D. Foust, *Energy Fuels*, 2014, **29**, 242–254.
22. A. Bridgwater, *J. Anal. Appl. Pyrolysis*, 1999, **51**, 3–22.
23. M. S. Mettler, A. D. Paulsen, D. G. Vlachos and P. J. Dauenhauer, *Energy Environ. Sci.*, 2012, **5**, 7864–7868.
24. R. Grout, K. Malhorta, P. Ciesielski, K. Gruchalla, B. Donohoe and M. Nimlos, *8th US National Combustion Meeting Organized by the Western States Section of the Combustion Institute*, 2013, #070CO-0341.
25. J. N. Reddy and D. K. Gartling, *The Finite Element Method in Heat Transfer and Fluid Dynamics*, CRC Press, 3rd edn, 2010.
26. O. C. Zienkiewicz, R. L. Taylor and P. Nithiarasu, *The Finite Element Method for Fluid Dynamics*, Butterworth-Heinemann, 2013.
27. P. Basu, *Biomass Gasification, Pyrolysis and Torrefaction: Practical Design and Theory*, Academic Press, San Diego, CA, 2nd edn, 2013, pp. 56,58.
28. E. Ranzi, M. Corbetta, F. Manenti and S. Pierucci, *Chem. Eng. Sci.*, 2014, **110**, 2–12.
29. A. Anca-Couce, R. Mehrabian, R. Scharler and I. Obernberger, *Energy Convers. Manage.*, 2014, **87**, 687–696.
30. A. Trendewicz, R. Evans, A. Dutta, R. Sykes, D. Carpenter and R. Braun, *Biomass Bioenergy*, 2015, **74**, 15–25.
31. C. Di Blasi and C. Branca, *Ind. Eng. Chem. Res.*, 2001, **40**, 5547–5556.
32. R. S. Miller and J. Bellan, *Combust. Sci. Technol.*, 1997, **126**, 97–137.
33. F. A. Agblevor and S. Besler, *Energy Fuels*, 1996, **10**, 293–298.
34. J. E. White, W. J. Catallo and B. L. Legendre, *J. Anal. Appl. Pyrolysis*, 2011, **91**, 1–33.
35. P. R. Patwardhan, J. A. Satrio, R. C. Brown and B. H. Shanks, *Bioresour. Technol.*, 2010, **101**, 4646–4655.
36. N. Kuzhiyil, D. Dalluge, X. Bai, K. H. Kim and R. C. Brown, *ChemSusChem*, 2012, **5**, 2228–2236.
37. R. Font, A. Marcilla, E. Verdii and J. Devesa, *Ind. Eng. Chem. Res.*, 1990, **29**, 1846–1855.
38. F. Thurner and U. Mann, *Ind. Eng. Chem. Process Des. Dev.*, 1981, **20**, 482–488.
39. C. Di Blasi, *Combust. Sci. Technol.*, 1993, **90**, 315–340.
40. A. M. C. Janse, R. W. J. Westerhout and W. Prins, *Chem. Eng. Process.*, 2000, **39**, 239–252.
41. K. Papadikis, S. Gu and A. V. Bridgwater, *Fuel Process. Technol.*, 2010, **91**, 68–79.
42. C. A. Koufopanos, N. Papayannakos, G. Maschio and A. Lucchesi, *Can. J. Chem. Eng.*, 1991, **69**, 907–915.

43. W.-C. R. Chan, M. Kelbon and B. B. Krieger, *Fuel*, 1985, **64**, 1505–1513.
44. A. G. Liden, F. Berruti and D. S. Scott, *Chem. Eng. Commun.*, 1988, **65**, 207–221.
45. A. K. Sadhukhan, P. Gupta and R. K. Saha, *Bioresour. Technol.*, 2009, **100**, 3134–3139.
46. G. M. Wiggins, P. N. Ciesielski and C. S. Daw, *Energy Fuels*, 2016, **30**, 4960–4969.
47. T. L. Bergman, A. S. Lavine, F. P. Incropera and D. P. Dewitt, *Fundamentals of Heat and Mass Transfer*, John Wiley & Sons, 7th edn, 2011, pp. 299–304.
48. S. V. Glass and S. L. Zelinka, *Wood Handbook: Wood as an Engineering Material*, Forest Products Laboratory, Madison, WI, 2010, pp. 4.1–4.19.

Fast Pyrolysis of Biomass
Advances in Science and Technology

Edited by

Robert C. Brown
Iowa State University, USA
Email: rcbrown3@iastate.edu

Kaige Wang
RTI International, USA
Email: kaigew@gmail.com

ROYAL SOCIETY OF CHEMISTRY

THE QUEEN'S AWARDS FOR ENTERPRISE: INTERNATIONAL TRADE 2013

Green Chemistry Series No. 50

Print ISBN: 978-1-78262-618-3
PDF eISBN: 978-1-78801-024-5
EPUB eISBN: 978-1-78801-186-0
ISSN: 1757-7039

A catalogue record for this book is available from the British Library

© The Royal Society of Chemistry 2017

All rights reserved

Apart from fair dealing for the purposes of research for non-commercial purposes or for private study, criticism or review, as permitted under the Copyright, Designs and Patents Act 1988 and the Copyright and Related Rights Regulations 2003, this publication may not be reproduced, stored or transmitted, in any form or by any means, without the prior permission in writing of The Royal Society of Chemistry or the copyright owner, or in the case of reproduction in accordance with the terms of licences issued by the Copyright Licensing Agency in the UK, or in accordance with the terms of the licences issued by the appropriate Reproduction Rights Organization outside the UK. Enquiries concerning reproduction outside the terms stated here should be sent to The Royal Society of Chemistry at the address printed on this page.

Whilst this material has been produced with all due care, The Royal Society of Chemistry cannot be held responsible or liable for its accuracy and completeness, nor for any consequences arising from any errors or the use of the information contained in this publication. The publication of advertisements does not constitute any endorsement by The Royal Society of Chemistry or Authors of any products advertised. The views and opinions advanced by contributors do not necessarily reflect those of The Royal Society of Chemistry which shall not be liable for any resulting loss or damage arising as a result of reliance upon this material.

The Royal Society of Chemistry is a charity, registered in England and Wales, Number 207890, and a company incorporated in England by Royal Charter (Registered No. RC000524), registered office: Burlington House, Piccadilly, London W1J 0BA, UK, Telephone: +44 (0) 207 4378 6556.

For further information see our web site at www.rsc.org

Printed in the United Kingdom by CPI Group (UK) Ltd, Croydon, CR0 4YY, UK